Simple Electromagnetic Motor Model for Torsional Analysis of Variable Speed Drives with an Induction Motor

T. P. Holopainen, A. Arkkio

Torsional vibrations must be considered in the design of all high-power drive-trains including an induction motor. Electromagnetic (EM) field in the air gap of an induction motor generates additional magnetic stiffness and damping between the rotor and stator. The inclusion of these magnetic effects is limited by the availability of simple and portable motor models. The main aim of this paper is to introduce a motor model including the speed and torque variation. The presented model is based on the linearization of the common space-vector models of induction motors. The parameters of this model are identified for the rated operating condition. This motor model can be extended to include variable speed and torque operation. The numerical results demonstrate that this model describes accurately the magnetic effects over the large speed and torque range. In addition, the numerical results demonstrate the significance of magnetic stiffness and damping in variable speed motor-driven compressors with a soft coupling.

1   Introduction

Induction motors rotate process machines by converting electric energy to mechanical work. The power is transmitted by a drive train including couplings and optional gears and branches. An essential part of the drive train design is the torsional vibration analysis. This analysis requires the inertia and stiffness data of all the drive train components with loading and damping parameters.

Increasing power density, together with increasing demands of reliability of industrial systems, has led to the increased requirements of calculation accuracy. With motor driven reciprocating compressors, this has resulted in the inclusion of magnetic stiffness and damping in torsional analysis (Anon., 2015). Due to this need, simple models, based on the motor characteristic data, have been presented for the evaluation of these magnetic parameters; see Knop (2012) and Hauptmann et al. (2013). These models are based on the space-vector theory, developed to describe the steady-state and transient motor behaviour, and used for the evaluation of magnetic stiffness and damping, see Concordia (1952), Jordan et al. (1979, 1980), Shaltou (1994) and Brunelli et al. (2015). Space-vector models, or the simplified versions of them, are well suited for the torsional analysis of drive trains. Using these models, the parameters required to describe the magnetic stiffness and damping can be calculated in advance by the motor manufacturer and submitted to the suppliers, e.g. compressor manufacturer, responsible for the drive train design.

Simultaneously, numerical methods have been increasingly applied for the analysis of induction motors. This trend has been expanded also to the determination of magnetic stiffness and damping parameters (Repo 2008) and the effect of these has been evaluated in calculation examples of actual drive trains (Holopainen et al. 2010).

The accuracy and modelling capability of numerical models exceeds clearly the potential of space-vector models. However, the accuracy is only one, though significant, requirement of feasible models for torsional analyses. A remarkable shortcoming of numerical models is the portability. The numerical models are usually non-linear and the application requires the integration of particular codes for electromagnetic fields. Thus, the portability of numerical motor models is poor, or at least limited. By contrast, the space-vector model is simple and the number of model parameters is small, and thus, the portability excellent.

The main aim of this paper is to introduce a simple linearized motor model including the speed and toque variation. The second aim is to show the significance of the magnetic stiffness and damping particularly in motor-driven reciprocating compressors with a soft coupling.

This paper is based strongly on the methods and findings of two previous papers, see Arkkio et al. (2016) and Holopainen et al. (2016). The paper starts by reviewing the linearization of the space-vector model in the operating point. Next, the inclusion of the speed and torque variation is presented. These two parameters define the steady-state operation of an induction motor. After this, the developed models are applied for a 3.7 MW induction motor. The obtained magnetic stiffness and damping values are compared to the results calculated numerically by a refined finite element (FE) method with time-stepping analysis. Finally, the motor model is applied to evaluate the magnetic effects on a reciprocating compressor drive train. All the calculations are carried out with a steady-state sinusoidal voltage supply of the motor. Thus, all the effects induced by the frequency converter control are neglected and the scope is restricted purely to the motor.

2 Methods

2.1 Space-vector Model of Induction Motor

A single-cage space-vector model for an induction motor written in a reference frame rotating at the synchronous angular speed ω_s is

$$
\begin{aligned}
\underline{u}_s &= R_s \underline{i}_s + \frac{d\underline{\Psi}_s}{dt} + j\omega_s \underline{\Psi}_s \\
0 &= R_r \underline{i}_r + \frac{d\underline{\Psi}_r}{dt} + j(\omega_s - \omega)\underline{\Psi}_r \\
T_e &= \frac{3}{2}p\,\mathrm{Im}\big(\underline{\Psi}_s^* \underline{i}_s\big)
\end{aligned}
\tag{1}
$$

where $\underline{u}_s$, $\underline{i}_s$ and $\underline{\Psi}_s$ are the space vectors of stator voltage, stator current and stator flux linkage, $\underline{i}_r$ and $\underline{\Psi}_r$ are the space vectors of rotor current and rotor flux linkage, R_s is the stator resistance, R_r is the rotor resistance, ω is the angular speed of the rotor, p is the number of pole pairs, j is the imaginary unit, and asterisk denotes complex conjugation. The angular speeds are given in electrical radians, i.e. $\omega = p\Omega$, where Ω is the mechanical rotational speed.

The linear relation between the flux linkages and currents is

$$
\begin{aligned}
\underline{\Psi}_s &= L_s \underline{i}_s + L_m \underline{i}_r \\
\underline{\Psi}_r &= L_m \underline{i}_s + L_r \underline{i}_r
\end{aligned}
\tag{2}
$$

where L_s and L_r are the self-inductances of the stator and rotor windings and L_m is the mutual inductance between them.

2.2 Linearization of Space-vector Model in Operation Point

The system of equations (1) is non-linear because of the product of angular speed and rotor flux linkage in the second equation. In addition, the electromagnetic torque in the third equation is non-linear due to the product of stator flux linkage and stator current. However, the torsional vibrations are manifested by small oscillations around the equilibrium point. Thus, the calculation of torsional vibrations can be carried out by linearizing the equations at the operation point. The linearized system of equations in the synchronously rotating reference frame is (Arkkio et al. 2016)

$$
\begin{aligned}
\Delta\underline{u}_s &= R_s \Delta\underline{i}_s + L_s \frac{d\Delta\underline{i}_s}{dt} + j\omega_s L_s \Delta\underline{i}_s + L_m \frac{d\Delta\underline{i}_r}{dt} + j\omega_s L_m \Delta\underline{i}_r \\
0 &= R_r \Delta\underline{i}_r + L_m \frac{d\Delta\underline{i}_s}{dt} + j(\omega_s - \omega_0)L_m \Delta\underline{i}_s + L_r \frac{d\Delta\underline{i}_r}{dt} + \\
&\quad +j(\omega_s - \omega_0)L_r \Delta\underline{i}_r - j\big(L_m \underline{i}_{s0} + L_r \underline{i}_{r0}\big)\Delta\omega \\
\Delta T_e &= \frac{3}{2}p L_m \mathrm{Im}\big(\underline{i}_{r0}^* \Delta\underline{i}_s + \underline{i}_{s0}\Delta\underline{i}_r^*\big)
\end{aligned}
\tag{3}
$$

where the currents have been chosen as the free variables, Δ denotes a small variation from the steady state value, i.e. a linearized variable, and $\underline{i}_{s0}$, $\underline{i}_{r0}$ and ω_0 are the steady-state stator current, rotor current and angular speed.

The resistance and inductance parameters of the non-linear and linearized space-vector models, (1) and (3), were obtained from a time-harmonic FE analysis (Repo et al. 2006). A non-linear effective permeability of operating point was used to get the parameters to calculate the steady-state currents of equation (1). A differential permeability was used to get the linearized parameters for equation (3).

2.3   Improved Space-vector Models

The simple space-vector model of equations (1) and (3) can be improved to include skin effect of rotor bars by increasing the number of rotor branches. Figure 1 shows a steady-state equivalent circuit having three rotor branches or cages. The corresponding dynamic space-vector model is (Arkkio et al. 2016)

$$
\begin{aligned}
\underline{u}_s &= R_s \underline{i}_s + \frac{d\underline{\Psi}_s}{dt} + j\omega_k \underline{\Psi}_s \\
0 &= R_r \underline{i}_r + \frac{d\underline{\Psi}_r}{dt} + j(\omega_s - \omega)\underline{\Psi}_r \\
0 &= R_q \underline{i}_q + \frac{d\underline{\Psi}_q}{dt} + j(\omega_s - \omega)\underline{\Psi}_q \\
0 &= R_p \underline{i}_p + \frac{d\underline{\Psi}_p}{dt} + j(\omega_s - \omega)\underline{\Psi}_p \\
T_e &= \frac{3}{2} p \, \mathrm{Im}\left(\underline{\Psi}_s^* \underline{i}_s\right)
\end{aligned}
\tag{4}
$$

where subscripts q and p refer to the second and third rotor branches. A double- and triple-cage linearized model can be constructed in a similar way as the single-cage model above. Again, the resistance and inductance parameters were obtained from a time-harmonic FE analysis (Repo et al. 2006)
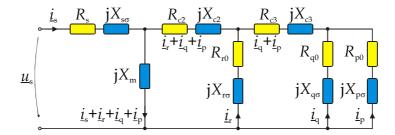

Figure 1. Steady-state space-vector equivalent circuit with three rotor branches (Arkkio et al. 2016)

The number of real-valued parameters, i.e. original and linearized model resistances and inductances, is 10, 18 and 26 in single-cage, double-cage and triple-cage models, respectively. The number of complex-valued variables, i.e. electromagnetic degrees-of-freedom, is 2, 3 and 4 in single-cage, double-cage and triple-cage models, respectively. Because the number of variables in a typical FE model used for the identification of parameters is thousands, the reduction grade is remarkable.

2.4   Variable Speed and Torque Operation

A large share of the new motors is used in variable speed applications. In these applications the motor speed and torque is adjusted according to process requirements. A common approach is to keep the fundamental flux of the machine constant independently of the actual speed and torque. This means that the supply voltage is directly proportional to the supply frequency up to the field weakening point, which is often above the maximum speed. It can be mentioned that modern frequency controllers may adjust the torque based on the feedback. However, all the calculations of this paper are carried out with a steady-state sinusoidal voltage supply of the motor, and thus, all the effects induced by the frequency converter control are neglected.

In this paper, the model parameters, i.e. inductances and resistances, are identified for the rated operating condition. These model parameters are extended to an arbitrary speed and torque by adjusting first the supply voltage according to the constant flux approach

$$\underline{u}_s = \frac{\omega_s}{\omega_{s,rat}} \cdot \underline{u}_{s,rat} \tag{5}$$

where the subscript "rat" refers to the rated values. The rotational speed and torque are connected by the slip of the rotor with respect to the rotating magnetic field

$$s = (\omega_s - \omega_0)/\omega_s \tag{6}$$

This slip must be solved iteratively from the non-linear equation (1) using the pre-set values of speed and torque. In addition, the inductances of the linearized model, equation (3), must be divided by the synchronous speed ratio $\omega_s/\omega_{s,rat}$. All other parameters of the non-linear and linearized models remain unchanged.

2.5   Calculation of magnetic Stiffness and Damping

The analytical expression for the frequency response function for the single-cage space-vector model is obtained from equation (3) by replacing the small variations by phasor variables of oscillation frequency ω_d and solving the relation between the torque and rotation angle of the rotor.

The magnetic stiffness k_m and damping coefficients d_m can be associated with the real and imaginary parts of the frequency response function $\underline{G}_{frf}$

$$\begin{aligned} k_m &= -\mathrm{Re}\big[\underline{G}_{frf}(\omega_d)\big] \\ d_m &= -\mathrm{Im}\big[\underline{G}_{frf}(\omega_d)\big]/\omega_d \end{aligned} \tag{7}$$

where ω_d is the angular frequency of oscillation.

2.6   Reference results by Finite Element Analysis (FEA)

In the 2D FEA models, the magnetic field in the core region of the motor is assumed to be two-dimensional. End-winding impedances are added to the circuit equations of the windings to approximatively model the 3D end-winding fields. The field and circuit equations are discretized and solved together (Arkkio 1990). Moving-band technique in the air gap of the machine is used for rotating the rotor (Davat et al. 1985). The torque is computed using Coulomb's method (Coulomb 1983). The resistive losses of the windings were included in the model when solving the field equations within FEA.

The frequency response function was needed for the reference result. Two time-stepping simulations in steady-state are used. In the first one, the rotor is rotated at a constant speed. In the second one, the rotation speed is forced to oscillate at a frequency ω_d and small amplitude around the constant speed of the first simulation. The results of the two simulations, particularly the electromagnetic torque and the rotation angle of the rotor, are subtracted from each other. The component varying at frequency ω_d is extracted from the torque and rotation angle differences by complex Fourier analysis, and finally, the complex value of the frequency response function at frequency ω_d is obtained by dividing the Fourier components of the torque and rotation angle. This process was repeated at about 30 different excitation frequencies between 10 Hz and 100 Hz to collect data for the comparison of the analytically and numerically obtained frequency response functions.

Another way to get the frequency response function numerically is to excite the machine by a single pulse in the rotation angle (Repo 2008). In this way, all the interesting frequencies can be obtained from two simulations, one with the pulse and another one without it. This method is applied to obtain the reference results for the variable speed and torque comparison.

3 Results

3.1   Magnetic stiffness and damping

A 3.7 MW induction motor is used in all the calculation examples. The main parameters of this motor are shown in Table 1.

Table 1. Rated parameters of the example motor.

Parameter	Value	Unit
Power	3551	kW
Frequency	60	Hz
Speed	895.3	rpm
Number or poles	8	
Connection	star	
Voltage	4000	V
Current	620	A
Rated torque	37.88	kNm
Breakdown torque	82.71	kNm

Figure 2 shows the magnetic stiffness and damping calculated by an analytic formula presented by Hauptmann et al. (2013), by single- and triple-cage models with parameters based only on the non-linear models, and FEA results. The FEA results are assumed to be most accurate and will be used here and later as reference values. In this case, the analytic equation underestimates the EM stiffness and damping and neglects the effects close to the supply frequency. Similarly, all the cage models underestimate the EM stiffness and damping. The triple-cage model gives the best prediction.
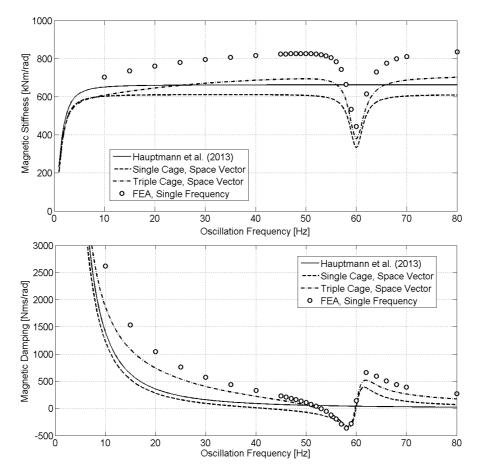

Figure 2. Magnetic stiffness and damping in rated operating condition with non-linear model parameters in cage models.
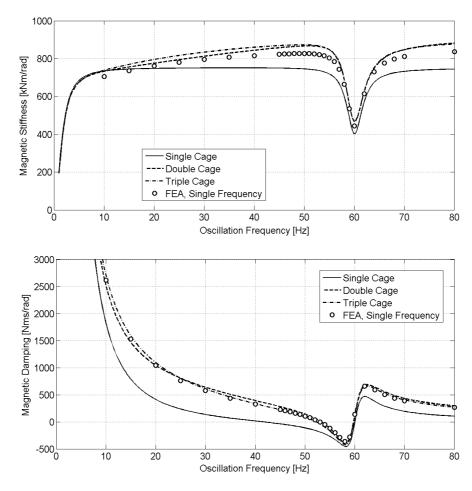
Figure 3. Magnetic stiffness and damping in rated operating condition with linearized space-vector model.

Figure 3 shows the magnetic torsional stiffness and damping in the rated operating condition calculated by linearized space-vector models and by FEA. The parameters of the space-vector models are identified for the slip frequency 1.2 Hz (Holopainen et al. 2016). As can be seen the single-cage model underestimates the stiffness and damping. In the contrary, the double- and triple-cage models overestimate somewhat the stiffness and predict the damping accurately. The difference between the double- and triple-cage models is small.

3.2 Effect of Speed and Torque

The synchronous speed range of the example motor in the variable speed operation is 450 – 900 rpm. This corresponds roughly to the supply frequency range 30 – 60 Hz. The field weakening point of this motor is at 60 Hz and the load torque of reciprocating compressors depends on the process medium and pressure ratio, and is independent of the speed. Thus, it is assumed that the torque varies between 50 – 100 % of the rated torque. Table 2 shows the calculation points. These points are the corner points of the speed-torque domain. However, for simplicity the calculation points are defined by the supply frequency and electric power. The slip, torque and speed values in table 2 are calculated by iteration during the space-vector and FEA solutions.

Figure 4 shows the magnetic stiffness and damping for these four operating points calculated by the linearized triple-cage space-vector model. It can be clearly seen that both the speed and torque affects the magnetic parameters.

Figure 5 shows the same information in the form of the complex frequency response functions (FRFs) between the torque and rotor oscillation, see equation (5). In this figure, the FRFs are plotted as functions of the relative oscillation frequency. This presentation format gives a better overview of the speed and torque effect on the magnetic stiffness and damping. It can be seen that the effect of speed (50% reduction) is slightly larger than the effect of torque (50% reduction). In addition, it can be seen that the change of torque changes the real part of the FRF, i.e. magnetic stiffness, but leaves the imaginary part of FRF, i.e. magnetic damping, almost intact.

Table 2. Calculated operation points of the example motor used in FEA.

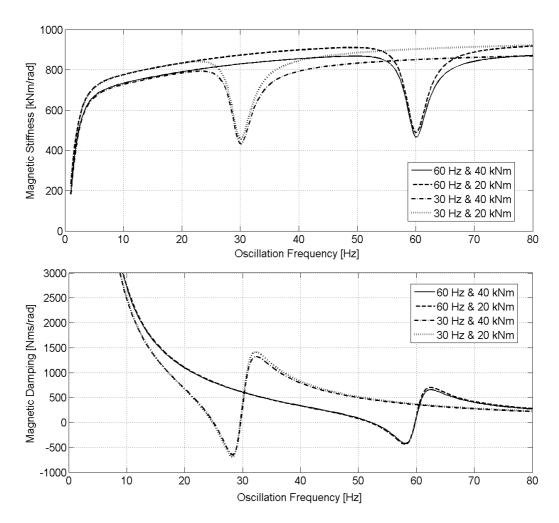| Case	Freq.	Power	Space-Vector Model			FEA		
			Slip	Torque	Speed	Slip	Torque	Speed
	[Hz]	[kW]	[%]	[kNm]	[rpm]	[%]	[kNm]	[rpm]
1	60	3729	0.546	39.78	895.1	0.543	39.78	895.1
2	60	1864	0.257	19.83	897.7	0.259	19.83	897.7
3	30	1864	1.114	40.01	445.0	1.108	40.00	445.0
4	30	932	0.518	19.88	447.7	0.521	19.88	447.7

Figure 4. Magnetic stiffness and damping calculated by the linearized triple-cage space-vector model.

Figure 6 shows the corresponding frequency response functions for the example motor calculated by the FEM in time domain and the pulse method (Repo 2008). It can be concluded that the behaviour of the linearized space-vector model (Figure 5) and the FE model (Figure 6) correlates well over the whole speed range.

3.3   Motor driven reciprocating Compressor

The example motor drives a reciprocating compressor. The drive train consists of the following components: Motor, flexible coupling, flywheel and reciprocating four-cylinder compressor. This compressor can be used in direct-on-line operation with constant speed 895 rpm and in variable speed operation (450 – 900 rpm) supplied by a frequency converter. The mechanical drive train was modelled with 26 inertias with connecting torsional stiffness elements. The viscous damping was added to the motor and compressor cylinder locations. The damping induced by the flexible coupling was neglected due to the missing input data.
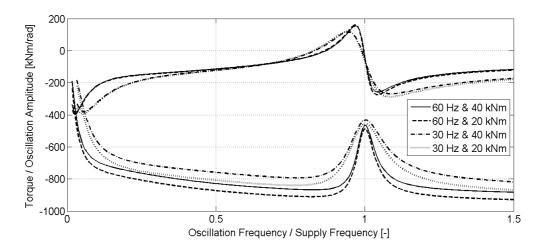
Figure 5. Frequency response function between the magnetic torque and rotor oscillation calculated by the linearized space-vector model. The real parts of the complex valued functions are below and the imaginary parts are up.
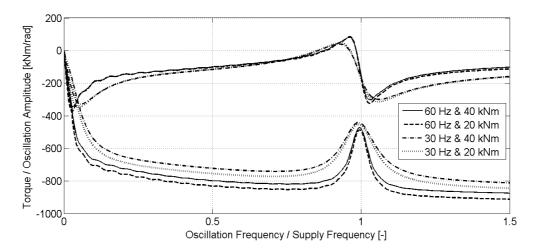

Figure 6. Frequency response function between the magnetic torque and rotor oscillation calculated by the FEA. The real parts of the complex valued functions are below and the imaginary parts are up.

Table 3 shows the natural frequency and damping ratio for the lowest modes without and with magnetic effects. The calculations are carried out by adding the magnetic stiffness and damping to the mechanical model. The calculation was carried out iteratively in order to use the magnetic stiffness and damping values corresponding to the natural frequencies. The first mode without magnetic effects is the rigid body mode. The main deformation of the second mode occurs in the flexible coupling. The third mode is an internal mode of the coupling, and in the fourth mode the flywheel and the compressor line are in the opposite phase without angular displacement of the motor.

Table 3 shows that the electromagnetic interaction increases clearly the natural frequency and damping ratio of the two first modes. The effect on modes 3 and 4 is negligible. This is logical due to the modal amplitudes of the modes 1 and 2 in contrast to the amplitudes of the modes 3 and 4.

Due to the variation of supply frequency, the magnetic stiffness and damping changes though the torque is assumed to be constant. Figure 7 shows the natural frequency and damping ratio of the two lowest modes as a function of the motor speed. In addition, the first and second order excitations are shown in this Campbell diagram. It can be seen that the natural frequency and damping ratios are only slightly dependent on the speed above 300 rpm. Below that speed the effects of the supply frequency on the second mode are clearly visible. Actually, the damping factor is negative in the speed rage 140 – 190 rpm. The second mode crosses the first order excitation frequency at about 600 rpm. The response of the system on this torsional critical speed depends on the first order excitation amplitude and the total damping. In this case the damping factor is predicted to be

8.6%. The amount of damping provided by the electromagnetic system is significant compared to the mechanical damping (Table 3).

Table 3. Natural frequency and damping ratio for the four lowest modes without and with electromagnetic coupling at rated operation.

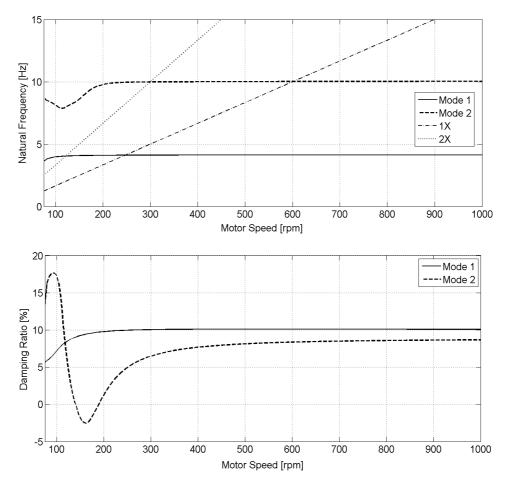| Mode	Magnetic Effects			
	Without		With	
	f [Hz]	ζ [-]	f [Hz]	ζ [-]
1	0.00	0.00	4.14	10.09
2	6.35	1.60	10.03	8.63
3	37.27	0.01	37.29	0.02
4	130.29	0.92	130.29	0.92

Figure 7. Natural frequency and damping ratio of the motor compressor train.

4 Discussion and Conclusions

The obtained results show that the linearized space-vector models can be used to predict the magnetic stiffness and damping of induction motors. Particularly, the prediction capability of the double- and triple-cage models in the rated operating condition is good. However, there seems to be a difference in magnetic stiffness compared to the FEA results. The triple-cage model yields about 5% higher stiffness values than the FEA. The origin of this discrepancy is not known.

The parameters of the presented non-linear and linearized space-vector models are obtained from the time-harmonic FEA. The number of parameters is 10, 18 and 26 in single-cage, double-cage and triple-cage models,

respectively. Because the number of variables in a typical FE model, used for the identification of parameters, is thousands, the reduction grade is remarkable. More importantly, the space-vector model is portable to be a part of standard torsional analyses without direct coupling to solvers of electromagnetic fields.

The calculation results indicate that the space-vector model can be extended to variable speed and torque operation. The results of the simple three-cage model are well compatible to the results obtained by the non-linear FEA in the time domain.

The calculation example for a reciprocating compressor train shows that the inclusion of magnetic effects is significant with flexible coupling. This follows from the two effects: The magnetic stiffness increases the natural frequencies and the magnetic damping decreases the oscillation amplitudes of torsional modes. The magnetic damping is particularly advantageous and can be exploited in the design of torsional drive trains.

The calculations were carried out with a steady-state sinusoidal voltage supply of the motor. Thus, all the effects induced by the frequency converter control are neglected and the scope is restricted purely to the motor.

References

Anon.: Guideline and recommended practice for control of torsional vibrations in direct-driven separable reciprocating compressors. *Gas Machinery Research Council, ACI Services*, (2015).

Arkkio, A.: Finite element analysis of cage induction motors fed by static frequency converters. *IEEE Trans. Magnetics*, 26, (1990), 551-554.

Arkkio, A.; Holopainen, T. P.: Space-vector models for torsional vibration of cage induction motors. *IEEE Trans. on Industry Applications*, 52, (2016), 2988–2995.

Brunelli, M.; Fusi, A.; Grasso, F.; Pasteur, F.; Ussi, A.: Torsional vibration analysis of reciprocating compressor trains driven by induction motors. In *Proc. 9th Int. Conf. on Compressors and their Systems*, London, UK, Sept.7-9, (2015), 10 p.

Concordia, C.: Induction motor damping and synchronizing torques. *AIEE Trans. Power Apparatus and Systems*, 71, (1952), 364-366.

Coulomb, J. L.: A methodology for the determination of global electromechanical quantities from a finite element analysis and its application to the evaluation of magnetic forces, torques and stiffness. *IEEE Trans. Magnetics*, 19, (1983), 2514-2519.

Davat, B.; Ren, Z.; Lajoie-Mazenc, M.: The movement in field modeling, *IEEE Trans. Magnetics*, 21, (1985), 2296-2298.

Hauptmann, E.; Howes, B.; Eckert, B.: The influence on torsional vibration analysis of electromagnetic effects across an induction motor air gap. In *Proc. GMRC Gas Machinery Conf.* Albuquerque, New Mexico, Oct. 6-9, (2013), 11 p.

Holopainen, T. P.; Repo, A.-K.; Järvinen, J.: Electromechanical interaction in torsional vibrations of drive train systems including an electrical machine. In *Proc. 8th IFToMM Int. Conf. Rotordynamics*. Seoul, Korea, Sept 12-15, (2010) 8 p.

Holopainen, T. P.; Liukkonen, O. J.; Arkkio, A.: Portable induction motor model for torsional vibration analysis of drive train systems. In *Proc. 11th Int. Conf. on Vibrations in Rotating Machinery*. Manchester, UK, Sept. 13-15, (2016), 141-151.

Jordan, H.; Müller, J.; Seinsch, H. O.: Über elektromagnetische und mechanische Ausgleichsvorgänge bei Drehstromantrieben. *Wiss. Ber. AEGTELEFUNKEN*, 52, (1979), 263-270.

Jordan, H.; Müller, J.; Seinsch, H. O.: Über das Verhalten von Drehstromasynchronmotoren in drehelastischen Antrieben. *Wiss. Ber. AEGTELEFUNKEN*, *53*, (1980), 102-110.

Knop, G.: The importance of motor dynamics in reciprocating compressor drives. In *Proc. 8th Conf. EFRC.* Düsseldorf, Germany, Sept. 27-28, (2012), 10 p.

Repo, A.-K.: *Numerical impulse response tests to identify dynamic induction-machine models*. Dissertation, Helsinki University of Technology, Finland, (2008).

Repo, A.-K.; Niemenmaa, A.; Arkkio, A.: Estimating circuit models for a deep-bar induction motor using time harmonic finite element analysis. In *Proc 17th Int. Conf. on Electrical Machines*, Chania, Greece, Sept. 2-5, (2006), 6 p.

Shaltout, A. A.: Analysis of torsional torques in starting of large squirrel cage induction motors. *IEEE Trans. Energy Convers.* 9, (1994), 135-142.

_____

Address: Timo P. Holopainen, ABB Oy, P.O. Box 186, FI-00381 Helsinki, Finland
email: timo.holopainen@fi.abb.com
                Antero Arkkio, Aalto University, P.O. Box 15500, FI-00076 Aalto, Finland
                antero.arkkio@aalto.fi